ADVANCED MATERIALS

Supporting Information

for *Adv. Mater.,* DOI: 10.1002/adma.202204890

4D Printing of Freestanding Liquid Crystal Elastomers via Hybrid Additive Manufacturing

Xirui Peng, Shuai Wu, Xiaohao Sun, Liang Yue, S. Macrae Montgomery, Frédéric Demoly, Kun Zhou, Ruike Renee Zhao, and H. Jerry Qi**

Supporting Information

4D Printing of Freestanding Liquid Crystal Elastomers via Hybrid Additive Manufacturing

Xirui Peng[1,2$], *Shuai Wu*[3$], *Xiaohao Sun*[1], *Liang Yue*[1], *S. Macrae Montgomery*[1], *Frédéric Demoly*[4], *Kun Zhou*[5], *Ruike Renee Zhao*[3*], *H. Jerry Qi*[1,2*]

[1]The George W. Woodruff School of Mechanical Engineering, Georgia Institute of Technology, Atlanta, GA 30332, USA
[2]Renewable Bioproduct Institute, Georgia Institute of Technology, Atlanta, GA 30332, USA
[3]Department of Mechanical Engineering, Stanford University, Stanford, CA, 94305, USA
[4]ICB UMR 6303 CNRS, Univ. Bourgogne Franche-Comté, UTBM, 90010 Belfort, France
[5]Singapore Centre for 3D Printing, School of Mechanical and Aerospace Engineering, Nanyang Technological University, 50 Nanyang Avenue, Singapore 639798, Singapore

[$]These two authors contributed equally to this work.

*Corresponding authors, Email: rrzhao@stanford.edu; qih@me.gatech.edu

Table of content

Supplementary Methods

UV-Vis characterizations The photoinitiators and dye are dissolved by IPA, and the solution is contained in cuvettes with a path length of 10 mm. The UV-vis absorption spectroscopy is obtained by a UV/Visible spectrophotometer (Ultrospec 2100 pro, GE Healthcare, Chicago, IL, USA) with an interval of 1 nm over the spectral region of interest.

Rheological property measurements The rheological properties of the LCE ink are measured using a rotational rheometer (Discovery HR-2, TA Instruments, New Castle, DE, USA) at 25 °C (using a 20-mm-diameter cross-hatched plate, gap height of 0.5 mm). Apparent viscosities are tested via steady-state flow experiments with a sweep of shear rates (0.1 - 400 s^{-1}). Shear storage moduli as a function of shear strain are measured by oscillation experiments at a fixed frequency of 1 Hz with a sweep of the strain of (0.02% - 5000%).

Measurement of the filament diameters The density of the bulky LCE ink is first measured by weighting a fine syringe before and after extruding a certain volume amount of LCE ink, which measured 1.215 g/cm^3. Then we assume that the density of the ink is constant with different printing parameters, and we assume that the LCE filaments are perfectly cylindrical. Then the diameter of the filament is calculated by $d = \sqrt{\frac{4w}{\pi L \rho}}$, where w is the weight of the filament, ρ the density, and L is the length of the filament.

Diameter variation To quantify the variation of the fiber diameters, we measured the diameter change along the fiber-direction directly through the photo of the fibers (Figure 2E) by Matlab. The original photo was cropped and transferred into grayscale, then the edges were detected using the Sobel method in MATLAB. Figure S8 shows the variation of the diameter along the fiber (printing) direction.

Gel fraction measurement LCE fibers are extracted in acetone for 10 days to characterize the GF of the networks. LCE fibers (40 mm in length) are printed at different speeds (four samples for each speed group). The weights of the fibers are measured before a week of extraction in acetone in 20 mL vials. After extraction, the samples are dried for 24 h in an oven at 80°C, and the weights are measured again. The GF is calculated by the following equation:

$$GF = \frac{w_f}{w_i} \times 100\%$$

where w_i is the initial weight and w_f is the dry weight after extraction.

Polarized optical microscope Leitz polarizing microscope by Martin Microscope Co. (Easley, South Carolina, USA) is used to observe the alignment of mesogens in the printed LCE. Images are taken by a Canon EOS6D camera with an LED light source. The light beam from the LED light source is polarized by a rotatable linear polarizer, and another linear polarizer is placed in front of the camera for parallel or cross polarization. As shown in Figure S5, three groups of images are presented, including the group with the analyzer parallel to polarizer, and two groups under cross polarization, with fiber direction oriented at 0° and 45° to the polarizer, respectively. By comparing the brightness of two groups under cross polarization, we can examine the mesogens' alignment in the fibers. In fibers printed by a low speed, the difference in brightness is small when the fiber is rotated, this indicates a small order parameter. With the increasing of the printing speed, the brightness change upon rotation is more obvious, indicating the increase of order parameter with the increase of printing speed.

Differential scanning calorimetry (DSC) DSC measurements are carried out using TA Instruments Q200 (New Castle, DE, USA). Samples are The samples sealed in the aluminum

pans are equilibrated at −30 °C and heated to 120 °C to erase thermal history, cooled to −30 °C, and then heated to 120 °C. The heating and cooling rate is 10 °C min^{-1}.

Dynamic mechanical analysis (DMA) DMA is performed using a dynamic mechanical analyzer (Model Q800, TA Instruments, New Castle, DE, USA). Samples (LCE fibers size: length 20 mm, diameter about 0.8 mm; Toughpoint sample size: 20mm × 3 mm × 0.2 mm) are first cooled to -50 °C and stabilized for 10 min to reach thermal equilibrium. A preload of 1 mN is applied, and the strain oscillates at a frequency of 1 Hz with a peak-to-peak amplitude of 0.1%. The temperature is increased from – 50 ℃ to 125 ℃ at a rate of 3℃ min^{-1}.

Hybrid Printing System

As shown in **Figure S16**, the hybrid printing system integrates the DIW system and the DLP system. The DLP projector (D912HD, Vivitek, Hoofddorp, Netherlands) with modified optics by B9Creator (Rapid City, SD, USA) is fixed above the printer frame with 3D motion stages, which is adapted from a commercial fused filament fabrication 3D printer (Ender 5, Shenzhen Creality 3D Technology Co., Ltd., Shenzhen, China). The printing substrate (50.5 mm × 75.5 mm glass slide with a black opaque film) is mounted on the z-motion stage, which is shared by both the DIW and the DLP systems. As the printing substrate travels down to the resin vat, light from the projector selectively cures the liquid resin. A lab jack is placed under the resin vat, and the height is calibrated, so that the ink surface in the vat is leveled at the zero position of the DLP system, at which the projector is focused. As the printing substrate travels to the upper range, all three motion stages work coordinately for freestanding DIW printing. The extrusion of inks in the syringe is pneumatically controlled by a dispenser (Ultimus I Nordson EFD, East Providence, RI, USA), and a pressure booster (HP10cc, Nordson EFD) is used to increase the pressure applied to the syringe. The laser curing module and the pressure booster (HP10cc, Nordson EFD) are mounted on the x-y-motion stage.

The light intensity of the projector is measured by a Radiometer Photometer (ILT1400-A, International Light Technologies Inc., Peabody, MA, USA). The light intensity of the DLP projector is about 10.5 mW/cm^2.

Finite Element Analysis

Finite element analysis (FEA) is performed to guide the structural designs for laser-assisted hybrid using the commercial software ABAQUS 2020 (Dassault Systemes, Vélizy-Villacoublay, France). Model dimensions, moduli and densities of LCE and inactive structures, orthotropic thermal expansion coefficients of the LCE fibers, and the applied temperature are the inputs to predict the thermal actuation of each design. For LCE fibers, a linear elastic model is used with Young's modulus of 1.4 MPa, Poisson's ratio of 0.49, and density of 1215 kg/m^3. Graded LCE fibers printed with different printing speeds (v_p = 30, 40, 50, 60 mm/min) show -19.1%, -23.3%, -29.3%, and -34.4% strain at 120 °C (reference temperature 20 °C) based on experimental measurements, and are modeled with four sets of orthotropic thermal expansion coefficients (See **Table S1** for details of the coefficients). For DLP printed rigid structures, a linear elastic model with Young's modulus of 1800 MPa, Poisson's ratio of 0.3, and density of 1215 kg/m^3 is adopted. The DLP printed flexible structures are modeled with a simplified linear elastic material with Young's modulus of 10 MPa, Poisson's ratio of 0.49, and density of 1215 kg/m^3. For simulations of LCE-embedded active lattices and pure LCE latices, element C3D8H is used. Three static steps are created, including applying the gravity, ramping up the structure temperature from 20 °C to 120 °C, and cooling the structure from 120 °C to 20 °C. For LCE active tensegrity and LCE actuator with tunable stability simulations, element C3D8R is used. Similarly, three steps of applying the gravity, heating the structure from 20 °C to 120 °C, and cooling the structure back to 20°C are simulated. Surface-to-surface contact (explicit) is used with conditions of finite sliding, frictionless, and hard contact. For the simulation of the LCE actuator with tunable stability, a half model is adopted to save the computational time, and two concentrated forces of 0.02 N and 0.013 N are applied to the top right and top left edges of the half model to represent the loading weights. For the LCE pyramid, a quarter model is adopted to

save the computational time for the three-step simulation, including applying the gravity, heating the structure from 20 °C to 120 °C, and cooling the structure back to 20 °C. For the graded LCE lattice printed under different printing speeds (v_p = 30, 40, 50 mm/min), three material models with different orthotropic thermal expansion coefficients (**Table S1**) are assigned to the model. The BCs of the standing feet are set as encastre, and the three-step simulation is also adopted.

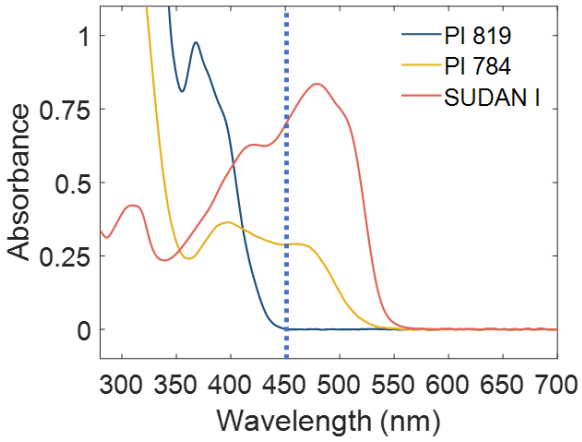

Figure S1. UV-Vis characterizations of different photoinitiators and photo-absorbers. The concentration of PI 819, PI 784, and SUDAN I in IPA are 0.05 wt%, 0.05 wt%, and 0.0018wt%, respectively.

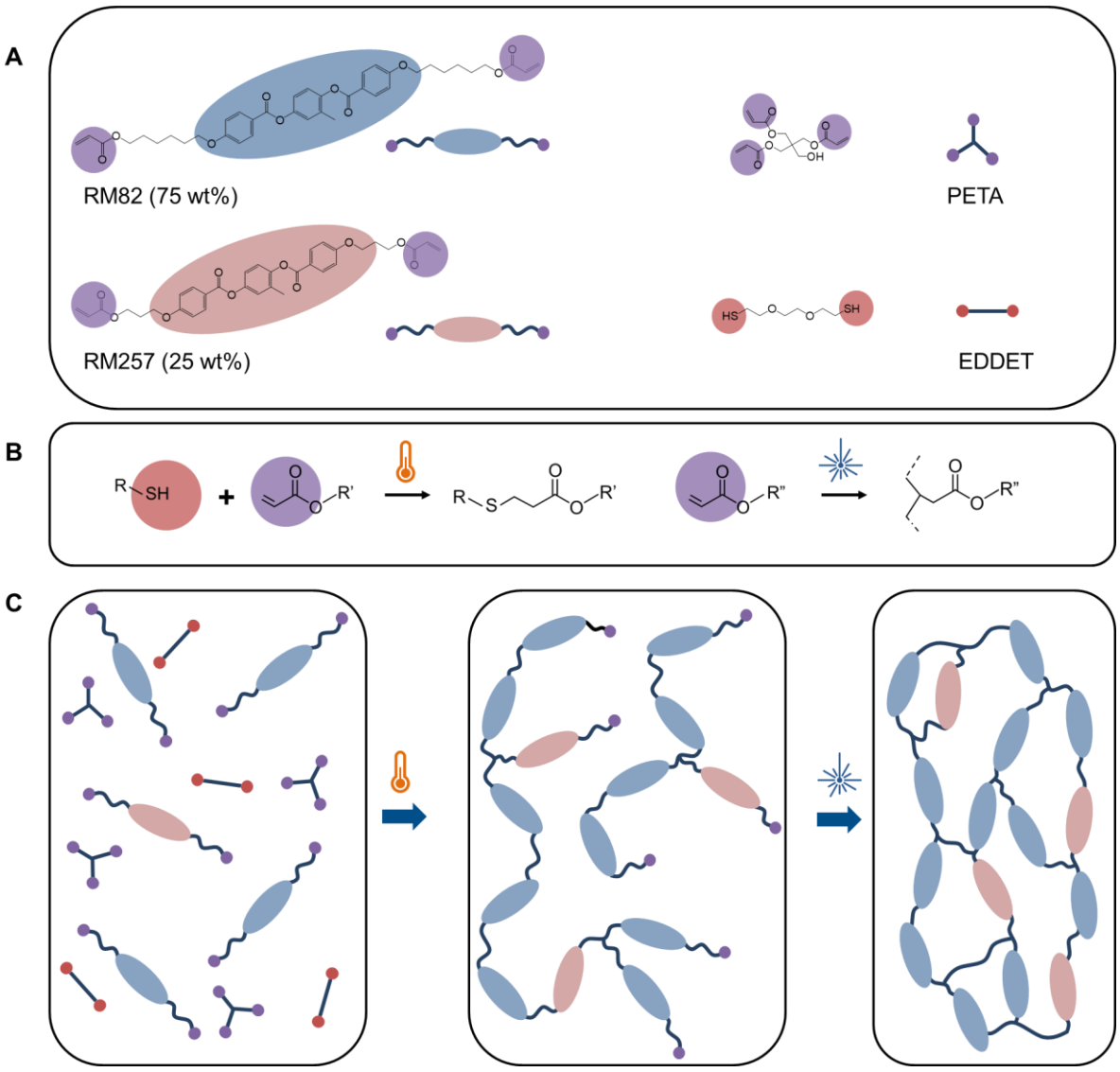

Figure S2. Two-step reaction of LCE ink. (**A**) The functional groups in the LCE components. The (**B**) reactions and (**C**) the schematics of the two-step reaction of LCE ink.

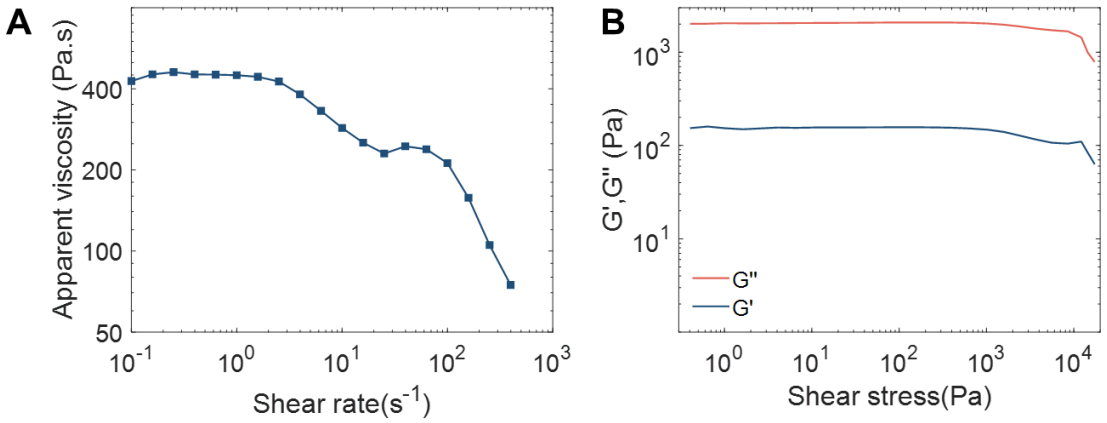

Figure S3. Characterizations of the LCE ink rheology. (**A**) Apparent viscosity of the LCE ink, showing shear thinning. (**B**) Shear storage and loss moduli of the LCE ink.

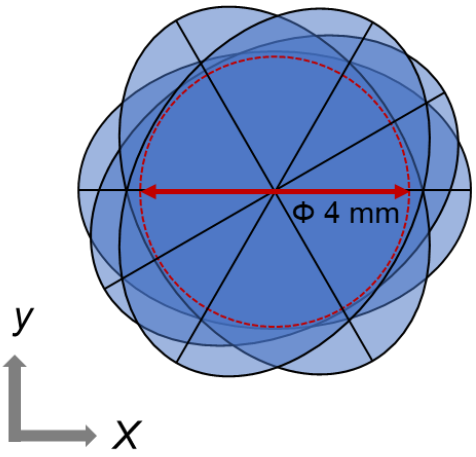

Figure S4. Schematic figure of the laser-beam pattern. The beams of four dot laser diodes (5 mW, 450 nm) are projected on the *xy*-plane, and the orientations of the semi-major axis of the elliptical areas are 0°, 30°, 60°, and 120° to the *x*-axis. The light intensity of the central area is ~112 mW/cm^2.

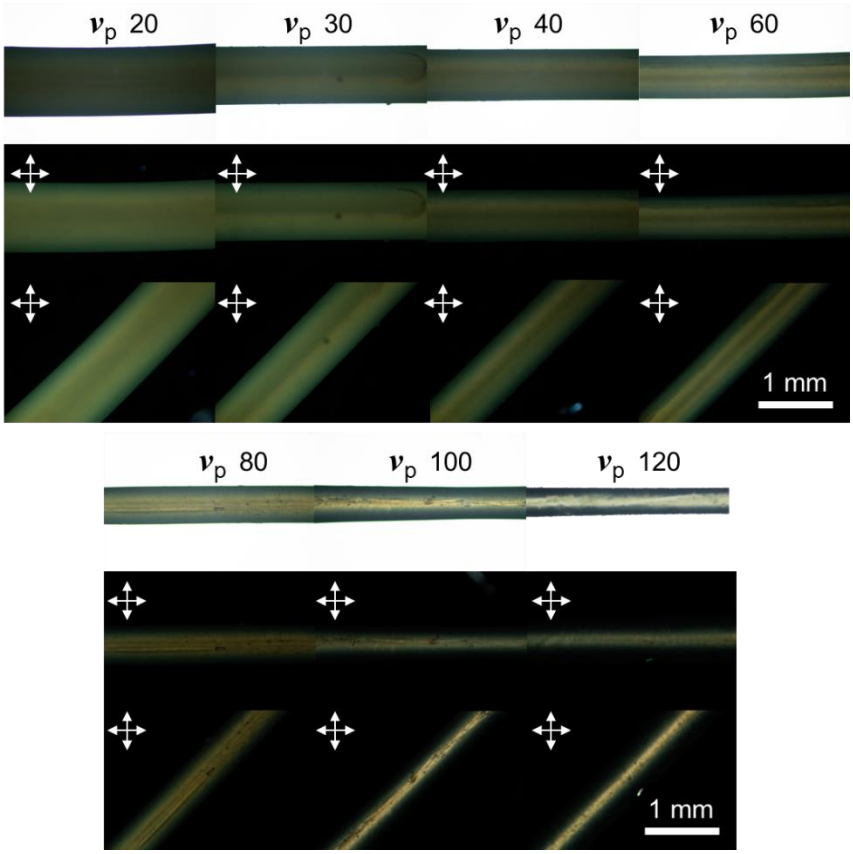

Figure S5. Polarized optical microscope (POM) images of LCE fibers with different printing speeds.

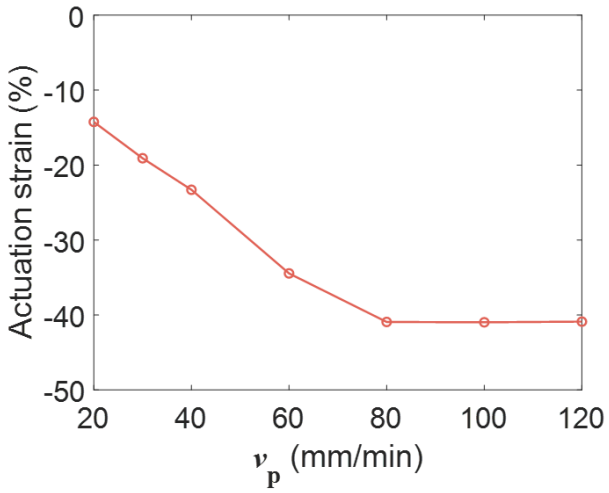

Figure S6. Comparison of the actuation strain of the LCE fibers printed with different speeds (60 psi, 20 Ga).

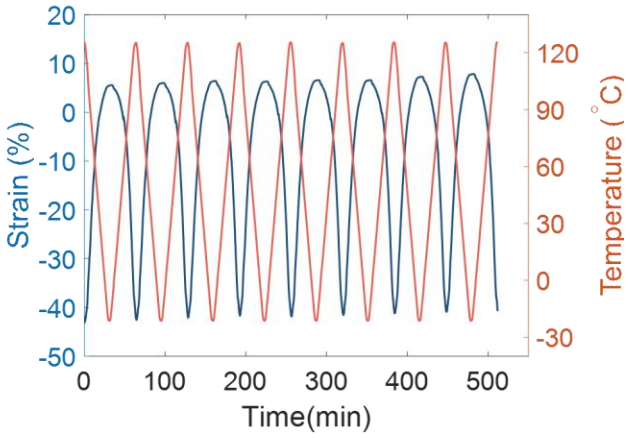

Figure S7. Actuation strain of the LCE fiber (vp 120 mm/min) upon cycling temperature. The temperature ramp rate is 5 ℃/min.

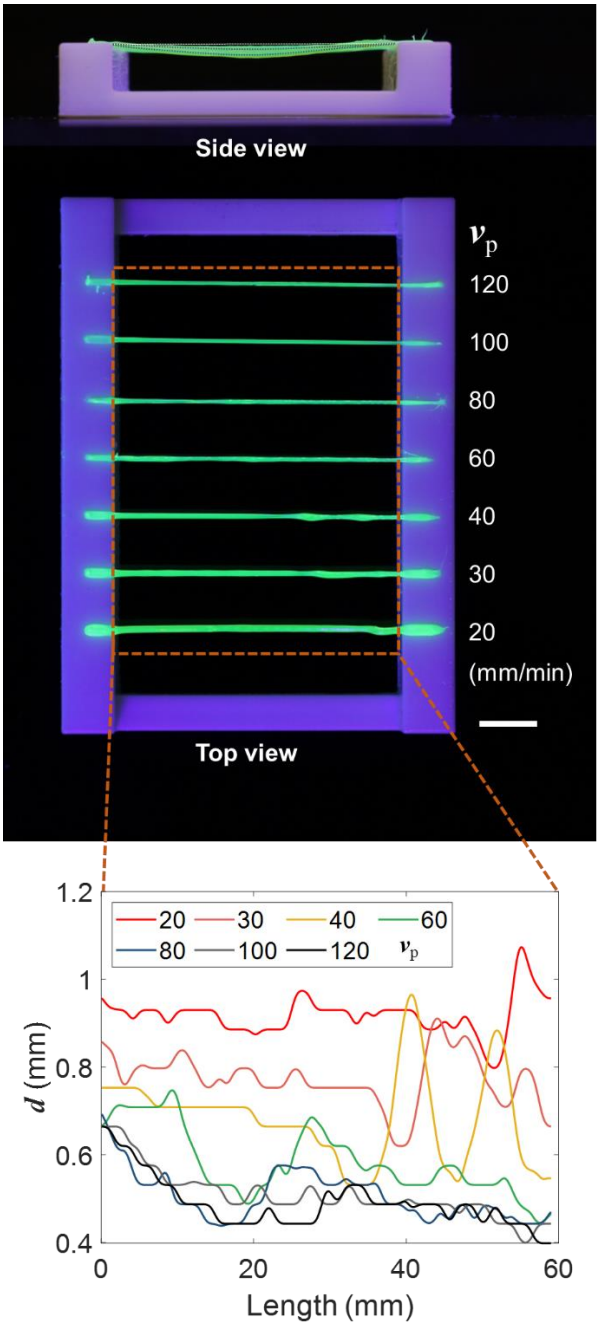

Figure S8. The side view, top view, and diameter variation of the LCE fibers printed at different speeds. The maximum central deflection of the fiber (20 mm/min, 50 mm span) is 2.11 mm. The standard deviation of the fibers' diameter ranges from 0.048 mm to 0.105 mm at different speeds. Thinning in fiber diameter is observed from fibers with higher printing speeds. Periodic fluctuations (e.g. fiber v_p 40 at length 35-55 mm) may occur due to the imperfections in printing condition. Scale bar: 10 mm.

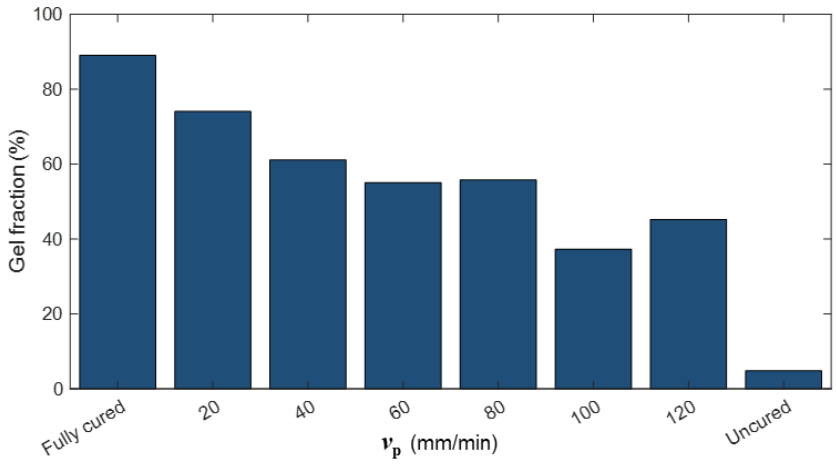

Figure S9. Gel fraction test of the fibers printed at different speeds without further post-curing.

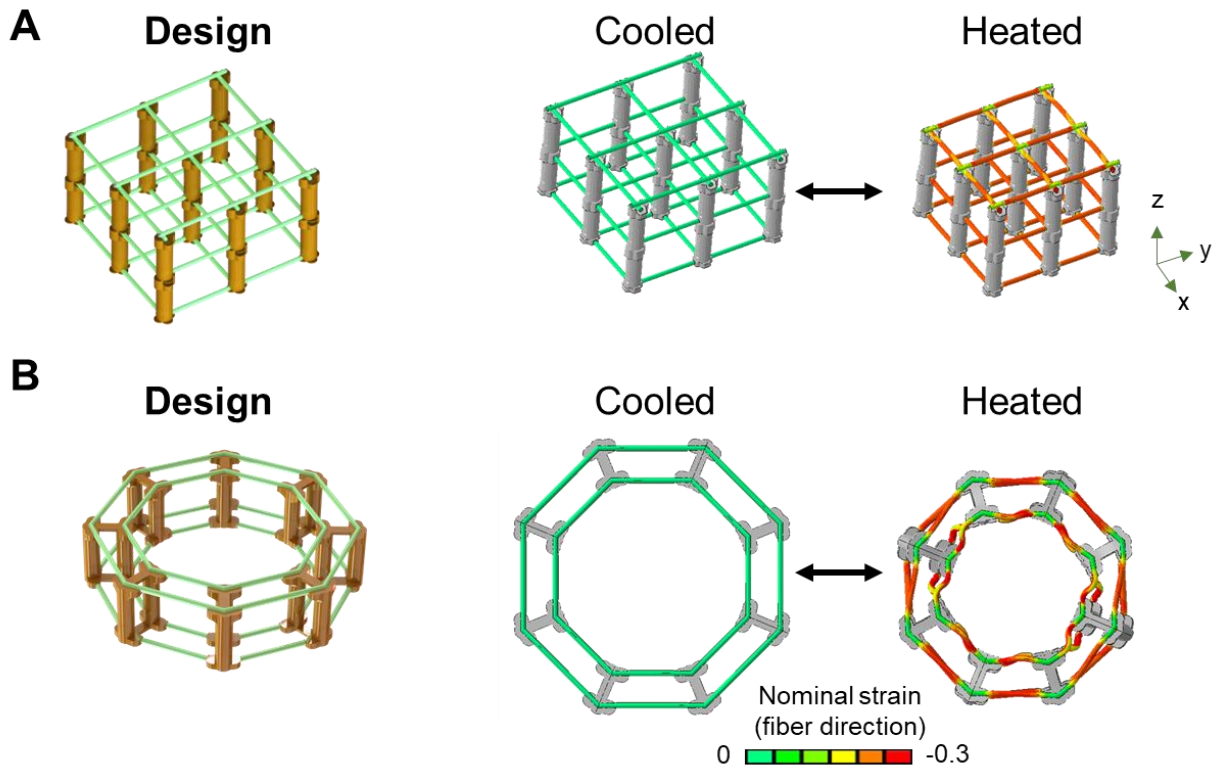

Figure S10. Finite element simulation of LCE-embedded active lattices. The design and LCE fiber nominal strain of (**A**) the hybrid cuboid lattice and (B) circular lattice at the initial and deformed configurations.

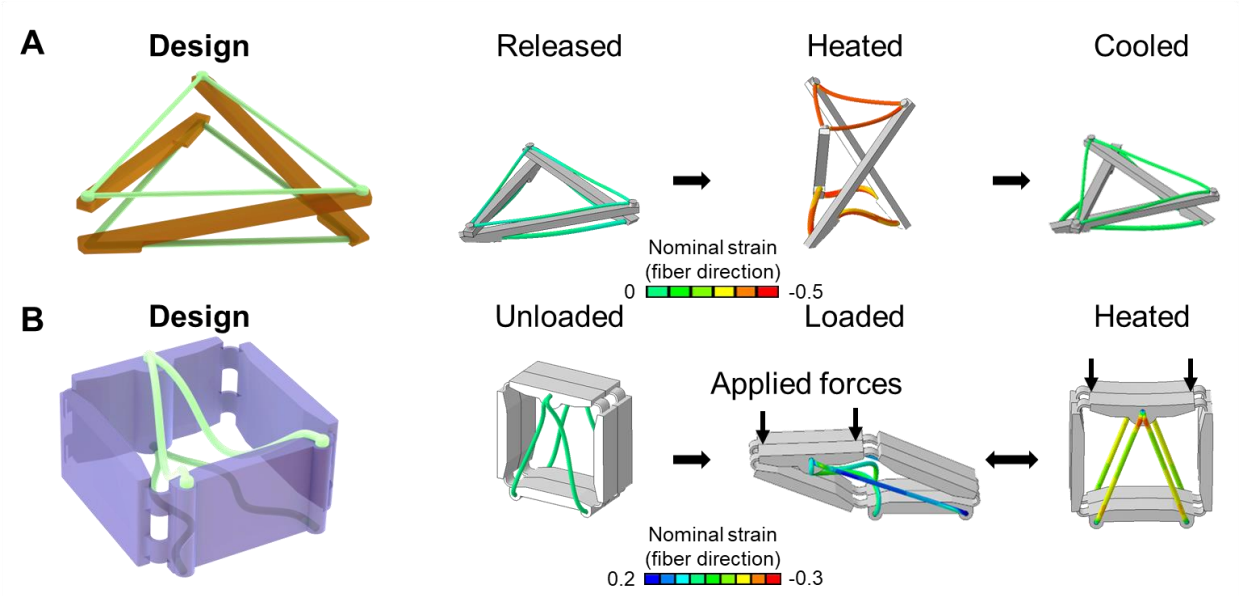

Figure S11. Finite element simulation of active tensegrity and actuator. The design and LCE fiber nominal strain of (**A**) the active tensegrity and (B) the actuator with tunable structural stability.

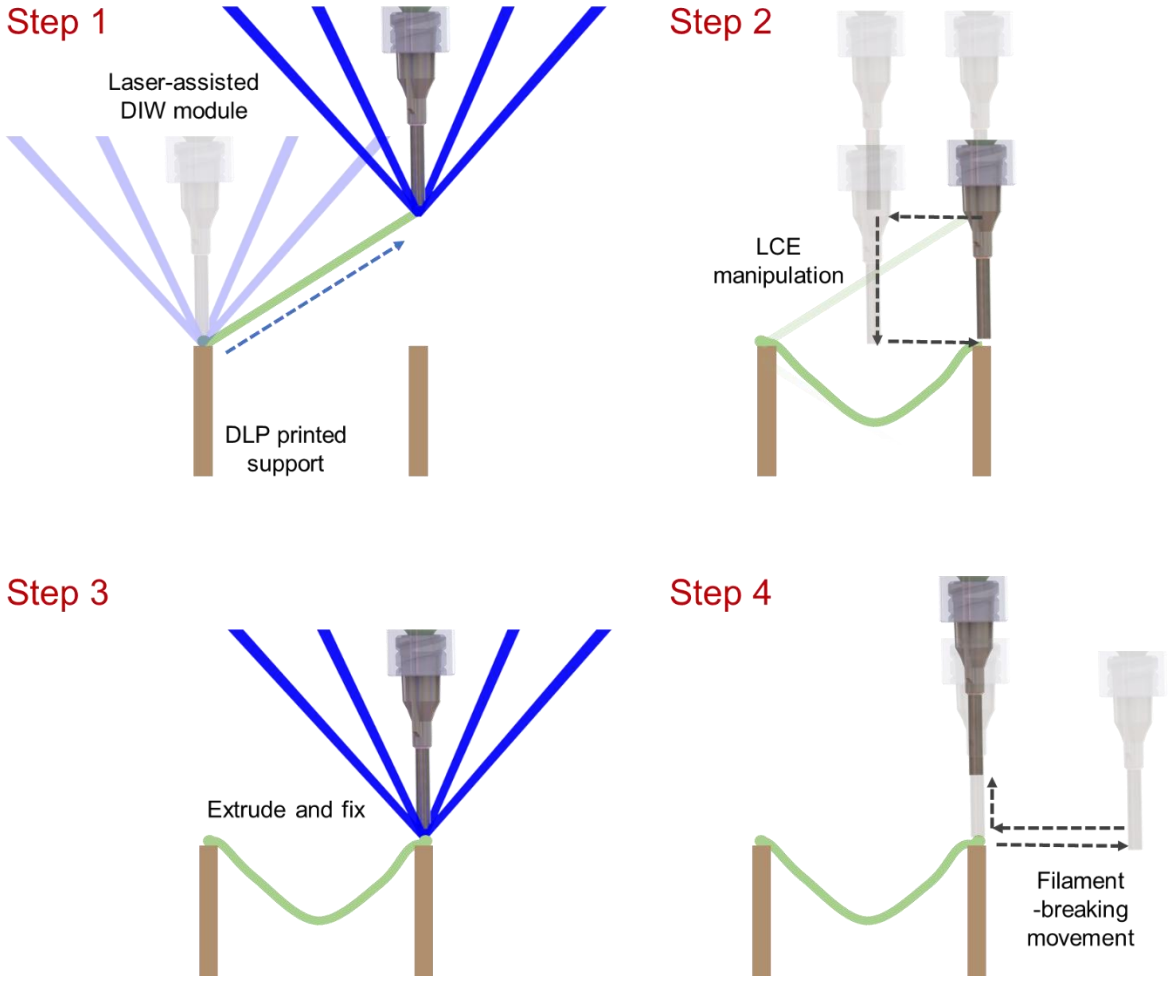

Figure S12. Printing procedures of relaxed LCE fibers with extra length. Step 1: Extrude with laser on and move towards a certain height above the destination point. **Step 2**: Stop extrusion and move the nozzle with a detour to manipulate the position of the LCE fiber. **Step 3**: Extrude with laser on to fix the endpoint of LCE fiber on the supporting structure. **Step 4**: Move the nozzle quickly to break the LCE filament and lift up the nozzle.

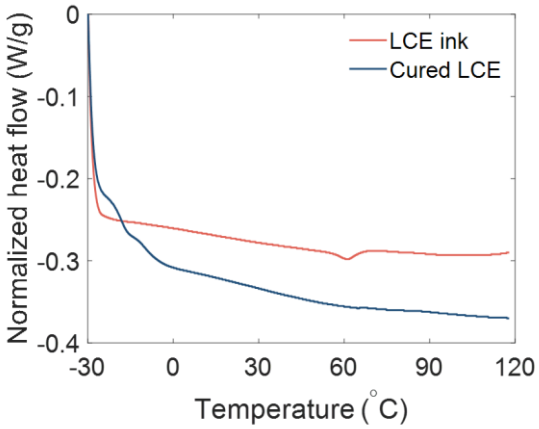

Figure S13. Differential scanning calorimetry (DSC) characterizations of the LCE ink and cured LCE.

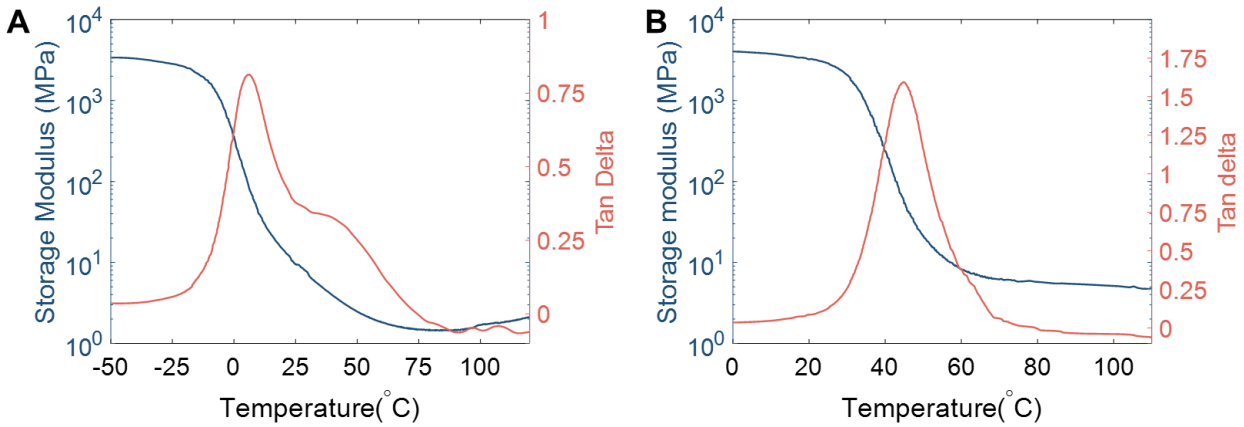

Figure S14. DMA characterizations. (A) Fully cured LCE; **(B)** The flexible structural material ToughPoint.

Figure S15. Polymerization of the soluble supporting ink (ACMO).

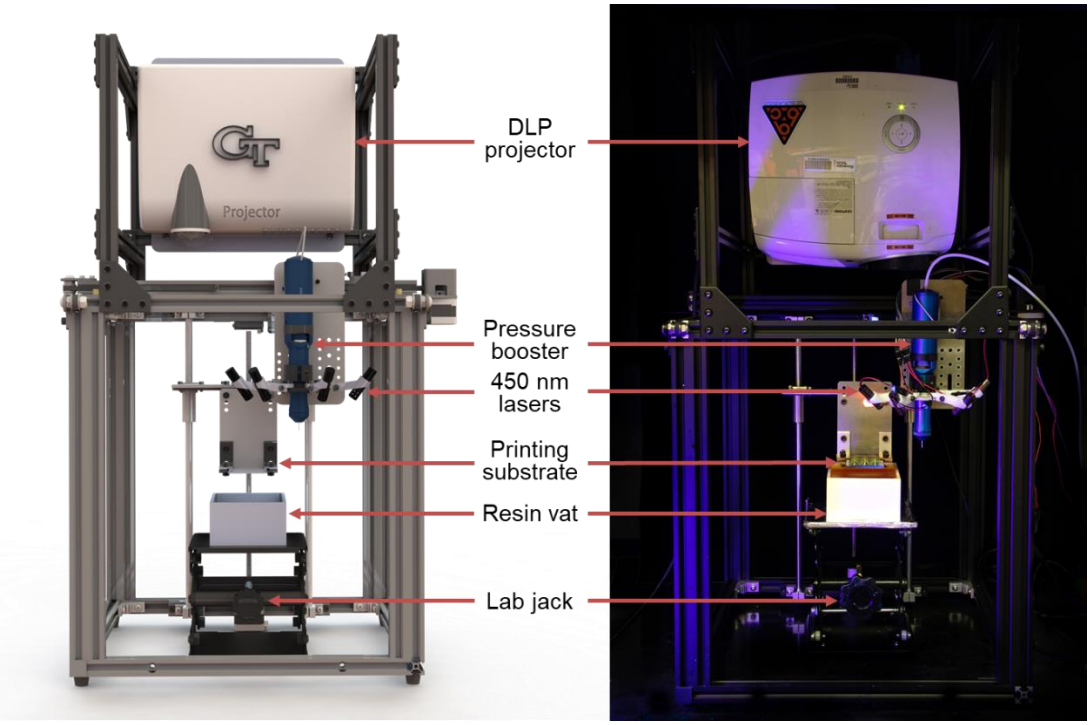

Figure S16. The design and actual photo of the hybrid printer.

Table S1. Table of coefficients of expansion used in FEA

Printing speed 60 mm/min

alpha11	alpha22	alpha33	Temp
0	0	0	0
-0.00247	0.001237	0.001237	20
-0.0035	0.001749	0.001749	40
-0.00487	0.002434	0.002434	60
-0.00424	0.00212	0.00212	80
-0.00344	0.001722	0.001722	100

Printing speed 50 mm/min

alpha11	alpha22	alpha33	Temp
0	0	0	0
-0.00211	0.001054	0.001054	20
-0.00298	0.00149	0.00149	40
-0.00415	0.002073	0.002073	60
-0.00361	0.001806	0.001806	80
-0.00293	0.001467	0.001467	100

Printing speed 40 mm/min

alpha11	alpha22	alpha33	Temp
0	0	0	0
-0.00168	0.000838	0.000838	20
-0.00237	0.001185	0.001185	40
-0.0033	0.001648	0.001648	60
-0.00287	0.001436	0.001436	80
-0.00233	0.001167	0.001167	100

Printing speed 30 mm/min

alpha11	alpha22	alpha33	Temp
0	0	0	0
-0.00137	0.000687	0.000687	20
-0.00194	0.000971	0.000971	40
-0.0027	0.001351	0.001351	60
-0.00235	0.001177	0.001177	80
-0.00191	0.000956	0.000956	100

The temperature in the table takes 20℃ as the reference 0 temperature.